WPS1-CPR(17) 17594

M Rack et al.

# Heat load re-distribution caused by manipulators on Wendelstein 7-X

Preprint of Paper to be submitted for publication in Proceeding of
643. WE Heraeus-Seminar

This work has been carried out within the framework of the EUROfusion Consortium and has received funding from the Euratom research and training programme 2014-2018 under grant agreement No 633053. The views and opinions expressed herein do not necessarily reflect those of the European Commission.

# On the design and operation restrictions of a probe manipulator for Wendelstein 7-X: a physicist' view

M. Rack,[1,2,*] D. Höschen,[1] D. Reiter,[1] B. Unterberg,[1] J. W. Coenen,[1] S. Brezinsek,[1] O. Neubauer,[1] S. Bozhenkov,[3] G. Czymek,[1] Y. Liang,[1] M. Hubeny,[1] Ch. Linsmeier,[1] and the Wendelstein 7-X Team

[1]*Forschungszentrum Jülich GmbH, Institut für Energie- und Klimaforschung – Plasmaphysik, Partner of the Trilateral Euregio Cluster (TEC), 52425 Jülich, Germany*

[2]*JARA-HPC*

[3]*Max-Planck-Institute für Plasmaphysik, 17491 Greifswald / 85748 Garching, Germany*

(Dated: October 5, 2017)

## Abstract

Probe manipulators are a versatile addition to typical plasma edge diagnostics. Equipped with material samples they allow for detailed investigation of plasma–wall interaction processes, such as material erosion, deposition, or impurity transport pathways. Combined with electrical probes a study of scrape-off layer and plasma edge density, temperature, and flow profiles as well as magnetic topologies is possible.

A mid-plane manipulator is already in operation on Wendelstein 7-X. A system in the divertor region is currently under development.

In the present paper, we discuss the critical issue of heat and power loads, power redistribution, and experimental access to the complex magnetic topology of Wendelstein 7-X. All aforementioned aspects are of relevance for the design and operation of a probe manipulator in a device like Wendelstein 7-X. A focus is put on the topological region that is accessible for the different coil current configurations at Wendelstein 7-X and the heat and power load on the manipulator with respect to the resulting, different magnetic configurations.

The qualitative analysis of power loads on plasma facing components is performed using a numerical tracer particle diffusion tool provided via the Wendelstein 7-X Webservices.



Keywords: stellarators, Wendelstein 7-X, manipulator, divertor, power load



*E-mail address: m.rack@fz-juelich.de

## I. INTRODUCTION

In magnetically confined fusion devices, an ideal extension to the typical plasma edge and material diagnostics is a probe manipulator in the plasma–wall interaction zone. Of specific interest is the high-heat-flux divertor region due to its comparatively high particle and energy fluence. An advantage of a manipulator is its capability for frequent exchange of test samples. In the process of developing and testing new plasma facing materials it allows: firstly, multiple materials and designs can be tested during the same experimental campaign without need to break the vacuum of the device; secondly, post-mortem analysis of samples can be performed right after the related experiments and samples do not get contaminated by other experimental conditions.

A comparable system was represented by the limiter lock at the Tokamak Experiment for Technology-Oriented Research (TEXTOR) [1], which was a "test limiter manipulator". It demonstrated excellent performance: quick exchange of material samples and high diagnostic coverage of the interaction zone. Besides material samples, a manipulator can be combined with electrical probes for the study of local scrape-off layer (SOL), plasma edge profiles and topologies. This provides further insight in the material exposed plasma.

A stellarator, such as Wendelstein 7-X, is geometrically more complex than a toroidal symmetric tokamak (like TEXTOR). Various different magnetic configurations are available in the former to change the location of the interaction zone. A toroidally varying cross-section combined with a limited number of available ports for a manipulator system restrict the accessible region. Furthermore, the plasma operation has to be guaranteed even without a material sample installed on the manipulator, which makes a quickly exchangeable entire divertor module like at ASDEX Upgrade [2] inappropriate.

This article focuses on the key aspects during the design and operation of a manipulator system in terms of three-dimensional magnetic topology, and heat and power load to plasma facing components. Therefore, the questions we address when analysing three different manipulator designs are: (a) can the material samples be placed such that they see an island divertor-like magnetic topology? (b) Is the heat flux in the interaction region controllable such that a limit in the order of $10\,\mathrm{MW\,m^{-2}}$ is not exceeded? (c) To what extent does the total heat load in the device get redistributed due to the insertion of a manipulator?

Two possible locations for a manipulator in the divertor region of Wendelstein 7-X are dis-

cussed. One already installed mid-plane manipulator system is analysed which also provides access to the divertor island, but up-stream.

Section II gives an overview on the geometrical manipulator set-up. In section III the field line tracing technique used for the analysis is introduced. The accessible topological region for the different set-ups is compared in section IV. A study on the heat and power load deposition onto the manipulator heads and resulting power load re-distribution for divertor components are presented in section V. Finally, the aforementioned observations are summarized in section VI.

## II. MANIPULATOR LOCATION

A consequence of Wendelstein 7-X' geometrical complexity is the limited space for accessing the divertor region by means of diagnostics. In addition, the permanent divertor components should not be modified for operation safety reasons. The two possible approaches of installing a manipulator in the divertor region that could be identified are: (a) accessing the divertor region through the pumping gap between the vertical and horizontal divertor target (section II A), and (b) acting as an extension of the horizontal divertor target at the low-$\iota$ end (typical strike-line location, section II B).

### A. Located in pumping gap

One option to enter the divertor region is through the pumping gap between the vertical and horizontal divertor plates. This location gives direct access to the high-heat-flux region at Wendelstein 7-X and allows to choose a toroidal location at which an excellent diagnostic coverage is provided via the installed endoscope and the attached diagnostics [3, Sec. 2.2]. The manipulator used within this design-study is located slightly above the horizontal divertor plate with the ability to propagate parallel to its surface in predominantly radial direction, see fig. 1. Its probe heads can have a vertical and toroidal extent of up to $3\,\mathrm{cm} \times 15\,\mathrm{cm}$ and can be equipped with material samples as well as electrical probes.

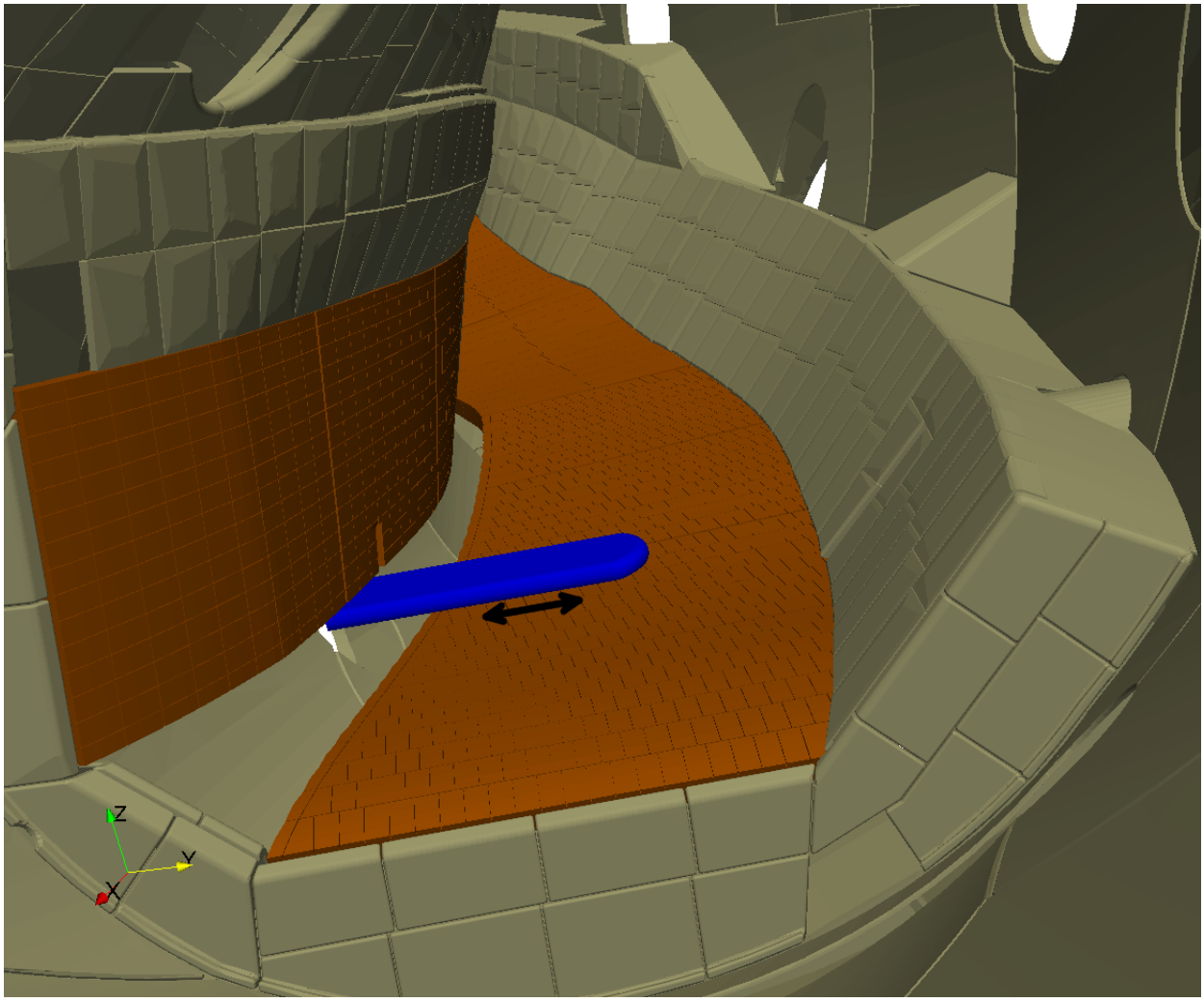


FIG. 1: Geometrical set-up of a divertor manipulator (blue) plunging into the plasma through the pumping gap. Divertor tiles are displayed in orange and additional wall components in grey. The black double-headed arrow indicates the movement direction of the manipulator. Here, the manipulator at deepest penetration is shown to present its maximum range. The shape of the probe head shape is not optimized and for this study a space holder.

### B. Horizontal target extension

Another option to enter the divertor region is through a port located at the bottom of the machine, toroidally in front of the low-$\iota$ end of the horizontal target, see fig. 2. It allows to move material samples from the shadowed region upward into the plasma–wall interaction zone. Consequently, magnetic field lines will have a similar incidence angle on the sample's surface as on the horizontal target itself which was optimized for minimum heat and particle

load. In this set-up, only a fraction of the typical divertor region (in radial direction) can be reached. Furthermore, the upward movement of samples is linked to a movement radially inward. This is due to the available port location which only allows a tilted insertion of the manipulator. The probe heads can have a radial and toroidal extent of up to 28 cm × 6 cm and can also be equipped with material samples and electrical probes.

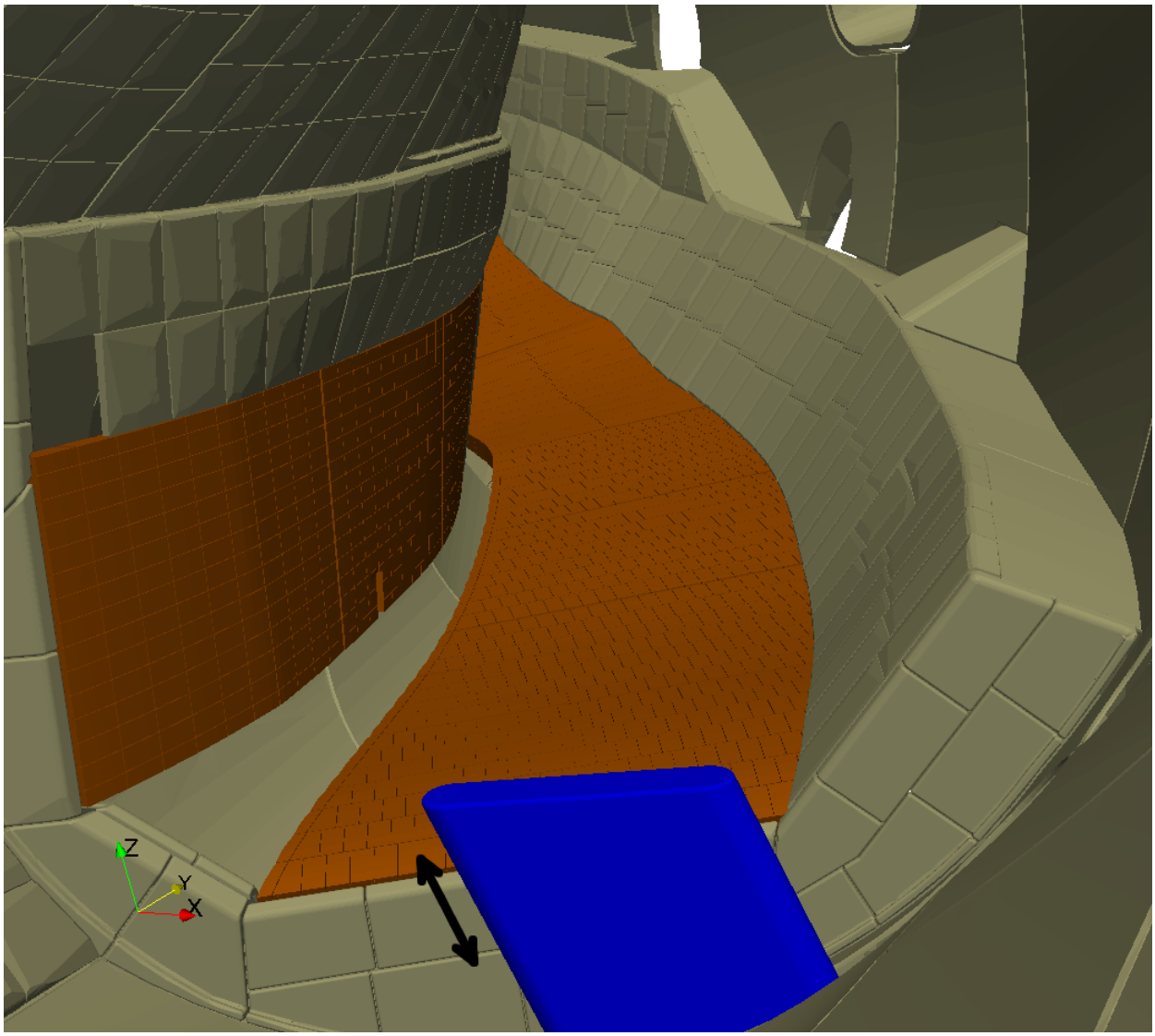


FIG. 2: Same as fig. 1 but for a divertor manipulator plunging into the plasma through a port in front of the low-$\iota$ end of the horizontal target.

Furthermore, the installation positions at the pumping gap and as a horizontal target extension presented here vary in the toroidal location due to the current availability of ports for implementing the system.

A drawback of the horizontal target extension is the need for setting up additional diagnostics at its location to observe and study the material exposure in real time. It cannot be observed with the already designed high resolution divertor observation systems.

### C. Located at outer mid-plane

In fig. 3 the set-up of the already installed manipulator [4, 5] at the outer mid-plane region is illustrated. It is located in a tear-drop-like cross-section and allows a nearly radial translation of probe heads for measurements, ranging from the far SOL up to several centimetres inside the confined plasma region. Equipped with electrical probes, the mid-plane manipulator can e.g. measure plasma properties inside the island chain [6]. Furthermore, material samples can be installed on the manipulator for plasma exposure with a maximum probe radius of 12 cm.

## III. FIELD LINE TRACING TECHNIQUE

The early design process of a manipulator system requires reliable but rapid feedback on the magnetic topology, and heat and power load seen by the manipulator. More detailed, but computationally costly, studies with code packages like the fluid edge plasma Monte-Carlo code in three dimensions (EMC3) [7] coupled to a kinetic neutral particle model EIRENE [8, 9] are part of a second stage, not covered within this work.

Here, a simple field line tracing technique is used. The location $\vec{r} = (R, \varphi, Z)$ of an individual magnetic field lines is described by

$$\frac{dR}{d\varphi} = R\frac{B_R}{B_\varphi}\,, \tag{1}$$

$$\frac{dZ}{d\varphi} = R\frac{B_Z}{B_\varphi}\,. \tag{2}$$

The three-dimensional magnetic field $\vec{B} = (B_R, B_\varphi, B_Z)$ itself is obtained by solving the Biot-Savart law for all electrical current carrying segments of the externally defined coil configuration. This allows to visualize in a simple manner the magnetic topology present in the region of interest. The connection length plots analysed in section IV have been produced by following magnetic field lines, started on a regular grid in an $R$-$Z$ plane at a fixed toroidal angle $\varphi$, in positive and negative toroidal direction until they intersect a wall

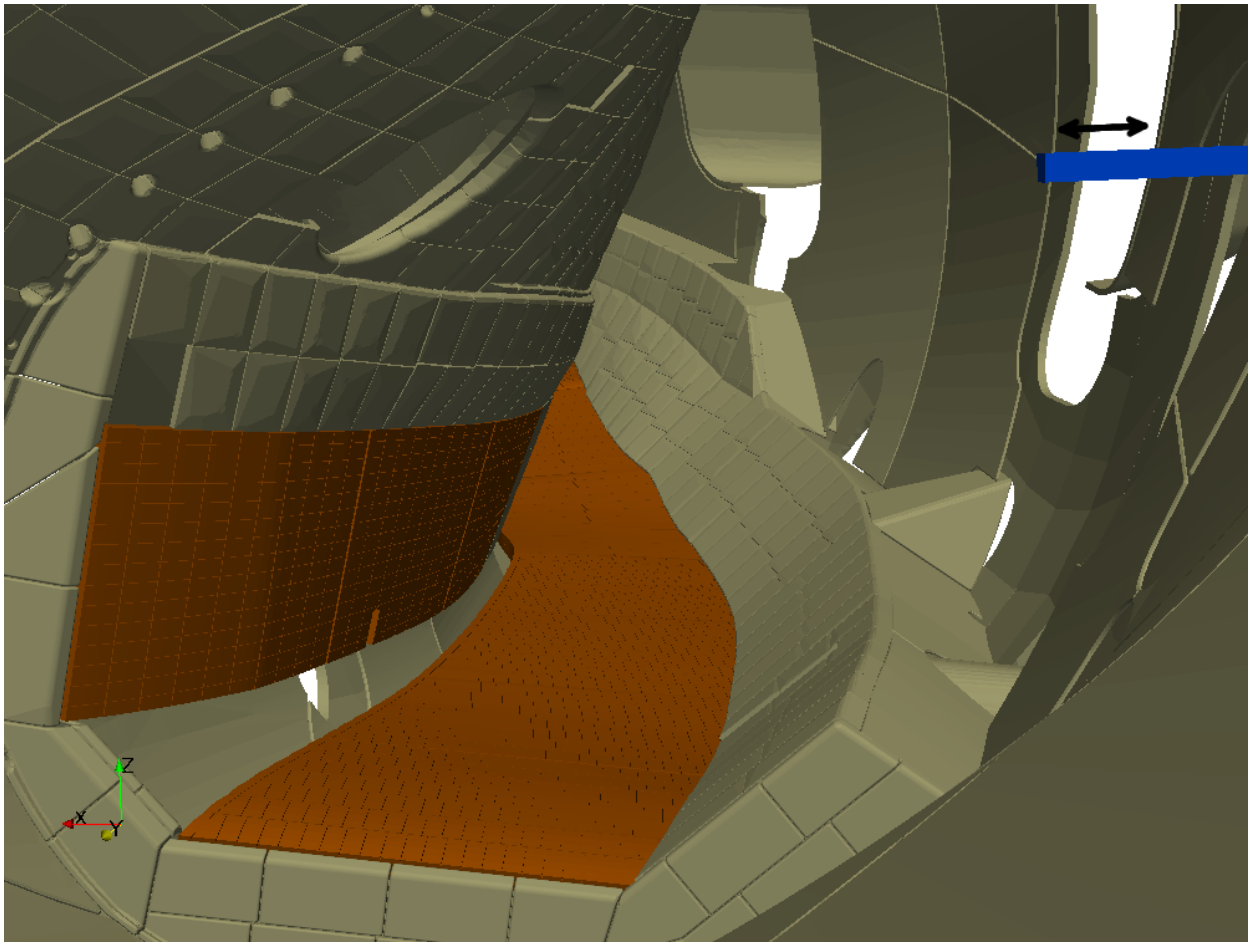


FIG. 3: Same as fig. 1 but for a mid-plane manipulator penetrating the plasma from the outboard side.

component. The connection length $L_C$ between the two intersection points is measured. Here, a maximum connection length $L_{C,max}$ need to be assumed above which field lines can be considered to have an infinite length. $L_{C,max} = 1\,\mathrm{km}$ appears sufficient for our Wendelstein 7-X cases discussed. Doing this, one can easily distinguish between regions of closed ($L_C = L_{C,max}$) and open ($L_C < L_{C,max}$) field lines. Furthermore, one can identify the magnetic islands and the separatrix location. Although more time consuming, this method brings advantages over a simple Poincaré plot as it allows to display the interaction region between plasma and wall in a sufficient way: one can easily differentiate between regions with and without plasma–wall contact, whereas a Poincaré plot only indicates the location and width of a magnetic island, see also [10, Sec. 3.2]. Figures in section IV present both, connection length plots and Poincaré plots, whereas the Poincaré plots are produced without

considering the divertor and wall components for providing a better representation of the magnetic island location.

With a simple extension one can even use the field line tracing approach to calculate rough estimates on heat transport from the confined region across the last closed flux surface (LCFS) onto the plasma facing components to deduce estimates of heat fluxes and power loads onto plasma facing components. A simple illustration of the method is given if we consider tracer particles to stream along the field lines. Such tracer particles carry a fraction of the total heating power and receive perpendicular kicks while travelling to simulate cross field transport in the plasma. In this simple model, tracer particles are started inside the LCFS and followed along and with a random, "diffusion-like" walk across field lines towards the targets. Each tracer particle carries a fraction of the total non-radiated heating power and is counted when intersecting the wall component which results in an estimate for the heat flux distribution to the plasma facing components. Effects arising from inertia terms, energy and momentum losses, volumetric heat sources, etc. are neglected here. Comparison of results from this model to full EMC3-EIRENE three-dimensional transport simulations, that account for the effects missing here, show an overestimation by about a factor of three to five towards higher heat fluxes predicted by the simple model. However, this accuracy is taken as sufficient for the elementary study presented here.

Here, we use the implementation in the "Field Line Tracer" of the Wendelstein 7-X Webservices [11]. This method has been applied earlier on Wendelstein 7-X for estimates of heat load distribution on divertor plates [12], characterisation of its edge region [13], and, recently, for feasibility studies of the scraper elements [14].

The considered plasma parameters $n$, $T$ in the SOL are taken as the averaged values of an EMC3-EIRENE reference calculation with a heating power of 10 MW, an up-stream density of $5 \times 10^{19}\,\mathrm{m}^{-3}$, and particle and heat diffusion coefficients of $1\,\mathrm{m}^2\,\mathrm{s}^{-1}$ and $3\,\mathrm{m}^2\,\mathrm{s}^{-1}$, respectively. Consequently, for the simple model used here: total heating power $P = 10\,\mathrm{MW}$ is kept the same, the averaged temperature derives to $T = 35\,\mathrm{eV}$, and the averaged density to $n = 1.5 \times 10^{19}\,\mathrm{m}^{-3}$. The cross-field thermal diffusivity $\chi_\perp = 3\,\mathrm{m}^2\,\mathrm{s}^{-1}$ is taken the same as the heat diffusion coefficient. Details of further input quantities can be found in the appendix.

## IV. MAGNETIC TOPOLOGY SEEN BY MANIPULATOR

A comparison of the magnetic topology created by the various magnetic configurations on Wendelstein 7-X reveals that very different plasma interaction zones can be reached by the manipulator system. The naming of the magnetic coil current set-up follows the IPP-Report by Andreeva [15]. We will only present selected magnetic configurations that are representative at the three different manipulator locations for reasons of brevity.

### A. Pumping gap

In the case of a manipulator in the pumping gap we can distinguish between two major scenarios: the manipulator enters the island through (a) the separatrix or (b) opened region; see fig. 4.

The figure for the standard configuration (top) shown here is representative for most of the reference configurations: high mirror, low mirror, inward shift, outward shift, low-$\iota$, and to some extent even low shear. As we will see below, the crossing of the island's separatrix before entering the region of interest is disadvantageous in terms of heat flux onto the manipulator head. Only in the high-$\iota$ case (bottom) the manipulator can enter the island without crossing its separatrix. By saying "separatrix", we mean the line of very long field lines defining the boundary of the island.

The low shear configuration is special as (due to the low shear) the island has a very small width, smaller than the manipulator head itself, which makes it difficult to enter the divertor island in the low shear case. In case of the limiter configuration the manipulator would act as the main limiter.

### B. Horizontal target extension

Considering a manipulator as a horizontal target extension at the low-$\iota$ end, we can separate the magnetic configurations into four groups: the manipulator (1) intersects only the interior of the island, (2) intersects the island and its separatrix, (3) intersects predominantly the separatrix, and (4) acts as the main limiter.

In fig. 5 examples from the first three groups (top to bottom) are presented. Here, the low mirror case (top) is also representative for the standard configuration with the given

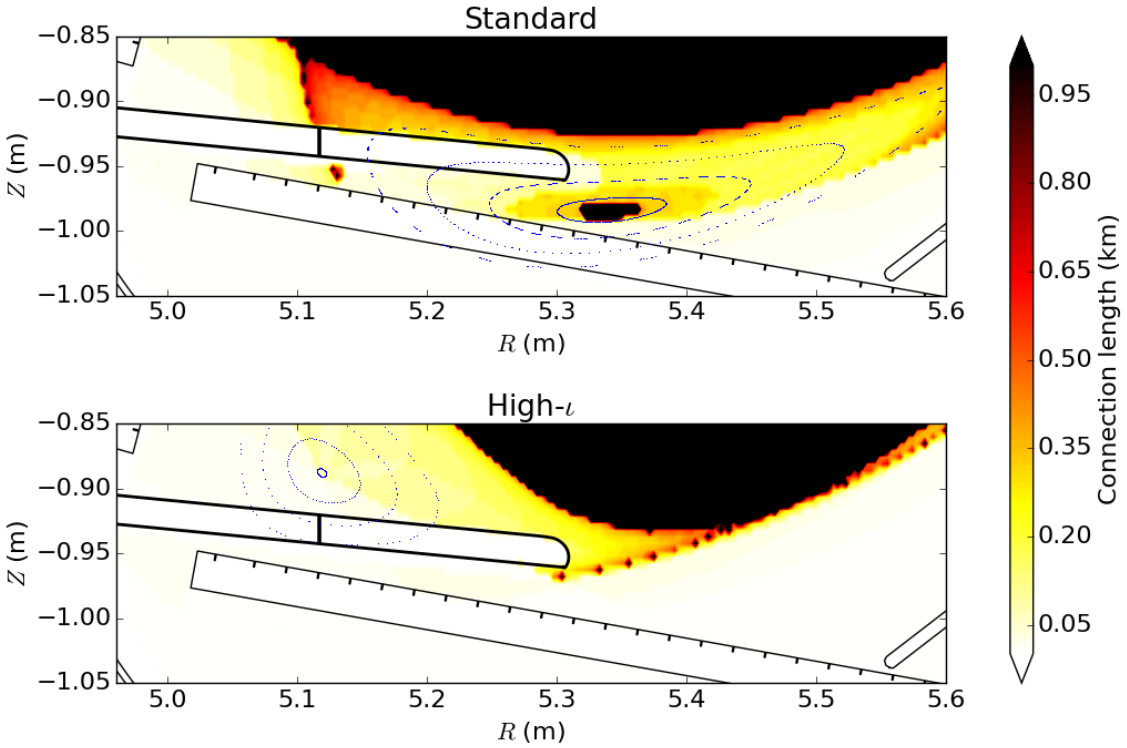


FIG. 4: Comparison of the magnetic topology as seen by a pumping gap manipulator in the case of the standard (top) and high-$\iota$ (bottom) configuration. The colour code represents the connection length of field lines at the various points in the poloidal cross-section shown. Solid lines indicate the location of wall components and the manipulator. A Poincaré plot is overlaid (blue dots) to indicate the presumably island location if no wall components are present.

shaping of the probe head. A special shaping allowing for an intersection with the separatrix would also enable the standard case to be listed in group (2). In contrast, the low mirror case shown here will always only allow access to the interior of the island due to a wider opening of the island. The high mirror configuration (middle) is representative for the largest group (including inward shift, low-$\iota$, and also outward shift). Even with different shaping of the manipulator head, an intersection with the separatrix is nearly inevitable. Only in the outward shift configuration one may reach a situation as in group (1), if required. Following from the different tilting of the island in the high-$\iota$ configuration (bottom) predominantly the separatrix will be intersected with the manipulator. Furthermore, the intersection happens very close to the confined region of the plasma which bears a certain risk to damage the probe. Same as above, in low shear and limiter configuration a manipulator at that location

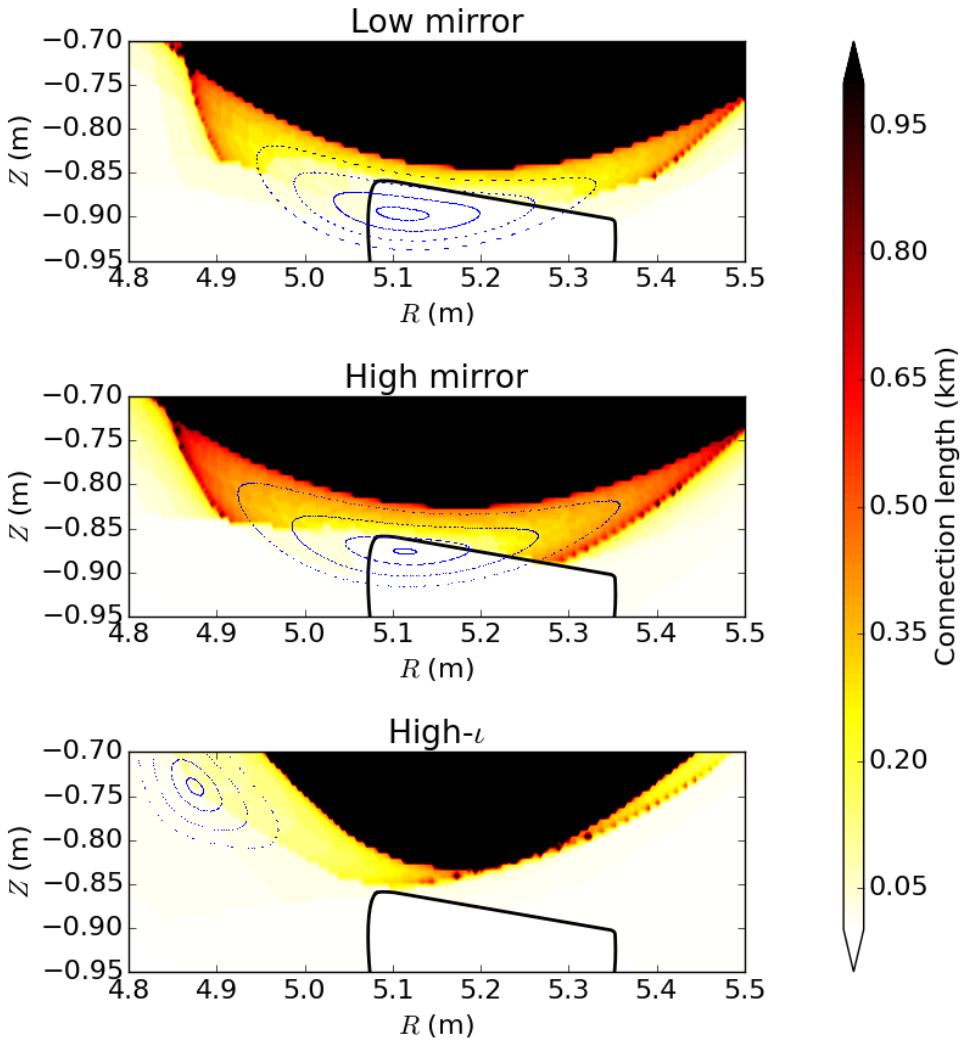


FIG. 5: Same as fig. 4 for the magnetic topology as seen by a manipulator acting as a horizontal target extension in the low mirror (top), high mirror (middle) and high-$\iota$ (bottom) configuration.

will act as the main limiter.

### C. Mid-plane

The installed mid-plane manipulator sees three different situations plus two limiter (like) cases. Depending on the magnetic configuration the probe head is (i) near the x-point of the island chain and needs to cross the separatrix to enter the island, (ii) near the o-point of island, and (iii) penetrates through a full open cut island. Figure 6 illustrates all three situations. Only in the low-$\iota$ configuration (left) situation (i) is present. The outward shift

configuration (middle) is also representative for the standard and inward shift configuration. The high-$\iota$ case (right) is representative for the low and high mirror configuration, as well. As before, in the low shear and limiter configuration the manipulator can act as a main limiter, only.

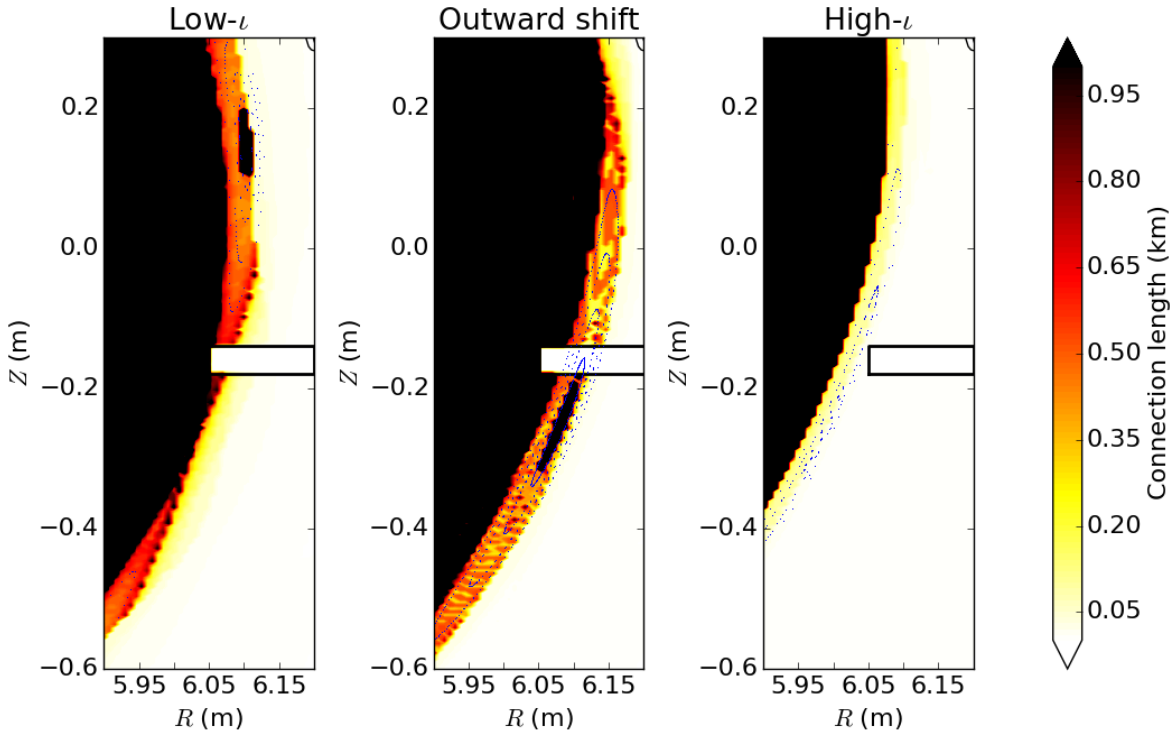


FIG. 6: Same as fig. 4 for the magnetic topology as seen by a manipulator located at the outer mid-plane the low-$\iota$ (left), outward shift (middle) and high-$\iota$ (right) configuration.

## V. POWER LOAD REDISTRIBUTION

The topological considerations above can give an overview of the reachable plasma zone for each manipulator set-up and magnetic configuration. However, it does not provide sufficient knowledge on the expected heat and power load onto the manipulator and the power load redistribution on the permanently installed divertor elements due to the inserted manipulator. Therefore, we make use of the model described in section III for estimates on the expected power load on the plasma facing components.

### A. Pumping gap

Comparing the estimated heat flux onto the plasma facing components in the standard configuration with and without the manipulator inserted through the pumping gap (fig. 7), one can observe two crucial changes. First, the heat load on the horizontal target reduces drastically when the manipulator is inserted. Second, the probe head of the manipulator receives a heat flux higher than the acceptable level of about $10\,\mathrm{MW\,m^{-2}}$ for damage-less operation. The most critical aspect in this manipulator set-up is the fact that leading edges cannot be avoided and, therefore, the surface peak heat flux cannot be reduced by shaping of the material samples. A peak heat flux of $100\,\mathrm{MW\,m^{-2}}$ on the horizontal surface of the manipulator and on the order of $1\,\mathrm{GW\,m^{-2}}$ at the leading edges have been estimated. Even when taking model uncertainties into account, this values are far above acceptable levels of current plasma facing materials.

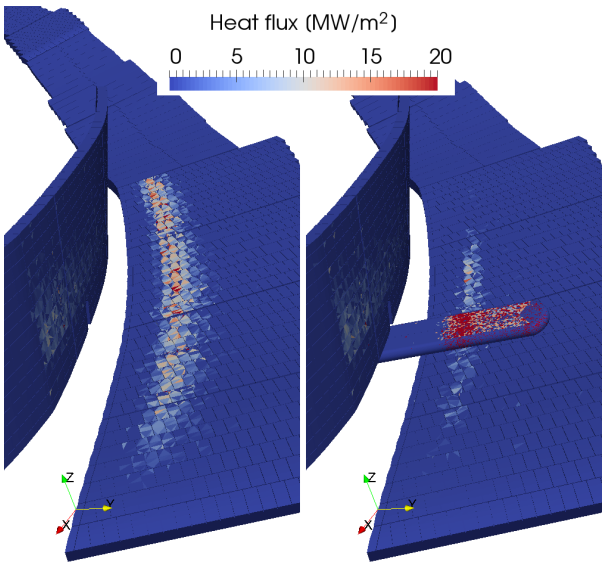


FIG. 7: Heat flux estimates in the standard configuration without (left) and with (right) pumping gap manipulator inserted into the divertor region. Here, only components that received heat load are displayed; see section II for a complete wall model.

In the numeric approach used, the power load (integrated heat flux) on components is the quantity known with highest accuracy. Therefore, we focus on comparisons of power loads rather than heat loads in the following. Furthermore, the integrated quantity power load per component is most usable for illustrating the comparisons of different configurations

and components and it provides the required information on whether a component will be overloaded or not.

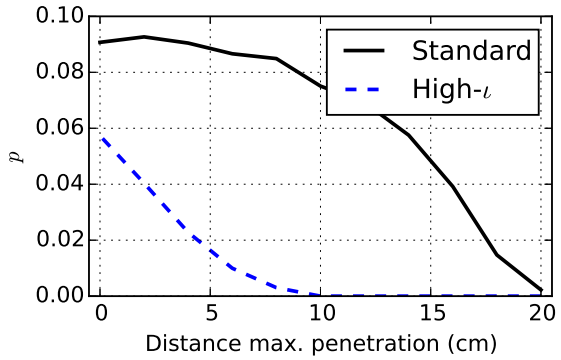


FIG. 8: Power fraction $p$ on pumping gap manipulator is compared for different penetration depth in the standard and high-$\iota$ configuration.

Figure 8 illustrates the differences in power load when inserting the pumping gap manipulator in a plasma confined by the standard and high-$\iota$ configuration. Power load is represented as the fraction of total power $P$ seen by the manipulator $p = P_{\text{target}}/P$. The position to which the manipulator is inserted is given as distance of manipulator tip from the maximum penetration depth that is still technically feasible. It only serves as a reference to compare the two configurations at different plunge depth. Key differences to observe are the increase to a power fraction of about 9 % several centimetres away from the maximum insertion position and the steeper gradient in the standard configuration. Recalling our observations in section IV A, the difference shown here appears obvious. It is a direct consequence from the fact that in the standard configuration the manipulator needs to cross the separatrix before entering the island. While doing so it receives the major fraction of power load and the interior of the island adds only a small fraction on top. In the high-$\iota$ configuration the situation is reversed which explains why the power load peaks at a much deeper position. Furthermore, the manipulator intersects the island to a much smaller fraction, only.

Exclusively in high-$\iota$ configuration one could place material samples at an acceptable location with heat and power loads sufficient low for a steady-state exposure. However, a perpendicular impact of field lines onto the manipulator head is unavoidable, independent of its shape.

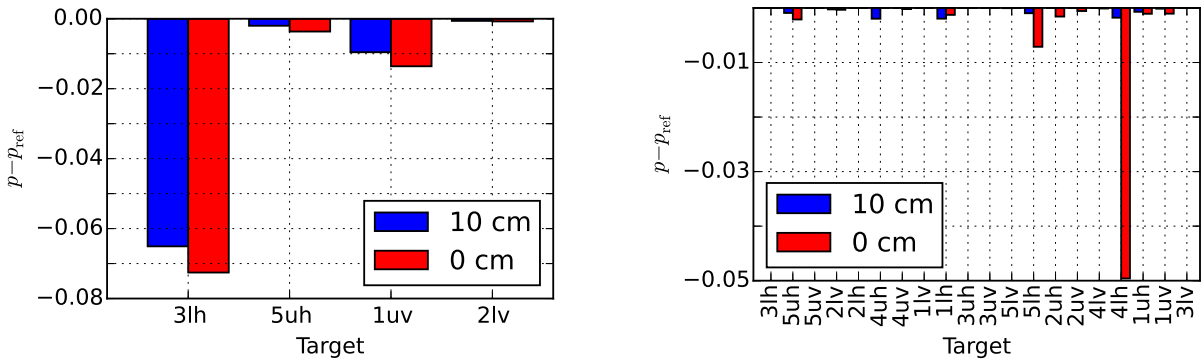


FIG. 9: Compares the change in power fraction on the target components for two different penetration depths of the manipulator. Standard (left) and high-$\iota$ (right) configuration are displayed here.

Figure 9 compares the power load redistribution due to the intersecting manipulator for a medium (10 cm) and full (0 cm) penetration in the case of the standard (left) and high-$\iota$ (right) configuration. The reference case $p_{\mathrm{ref}}$ is obtained without the manipulator. Divertor targets are abbreviated using the following syntax **#ab**:

**#** Wendelstein 7-X module number,

**a** upper (u), or lower (l) divertor,

**b** vertical (v), or horizontal (h) target.

Only targets seen by the perturbed island are displayed and its ordering along the x-axis follows the helicity of the magnetic island starting from the manipulator location.

In most magnetic configurations at Wendelstein 7-X the five divertor islands are independent, only in the high and low-$\iota$ configurations one island exists. Consequently, the intersected island connects to only four of the 20 divertor targets in case of the standard configuration and to all 20 targets in the high-$\iota$ configuration. In standard configuration we know from fig. 7 already that the load in the same divertor module (3) gets strongly reduced when inserting the manipulator. Figure 9 (left) confirms that the manipulator shadows nearly all power flux to the lower horizontal divertor in the same module. A smaller fraction (about 1 % of the total heating power) gets shadowed from the upper vertical target in module 1. This effect is not only seen for the full penetration (0 cm) but also at a medium

penetration (10 cm); see discussion above. Again, the standard configuration is representative for majority of magnetic configurations. Only, depending on plasma shift, a stronger power load reduction on upper vertical target in module 1 can be observed.

The results in the high-$\iota$ configuration differ. On the one hand, a significant reduction of power load on the divertor targets is only seen when fully inserting the manipulator (consistent with fig. 8). On the other hand, the reduction appears at a remote location, in module 4. Following the magnetic island, this is 4/5 turns apart from the interaction region of the manipulator. When performing experiments with such a manipulator, one needs to be aware of this property to have an additional control parameter for the power load on the manipulator by viewing the remote locations.

One possibility to reduce heat loads onto the pumping gap manipulator is the design of a new magnetic configuration which places the plasma strike-line smoothly on the horizontal sample surface. However, this is on the one hand prone to inaccuracy due to plasma instabilities and on the other hand significantly more difficult than the second option discussed here which make use of exactly this property in a more protected area.

### B. Horizontal target extension

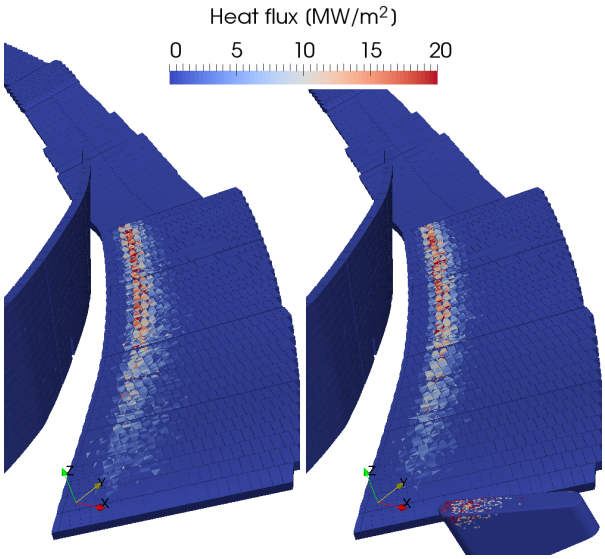


FIG. 10: Same as fig. 7 in the low mirror configuration for the horizontal target extension manipulator.

Comparing the heat flux distribution on the horizontal target extension manipulator (fig. 10) with the pumping gap manipulator (fig. 7) one can notice a much lower peak heat flux on the probe head. Furthermore, the heat is distributed over a wider radial range and leading edges are mostly avoided. Additional optimisation may be achieved via improved shaping of the probe head. Furthermore, we can notice a much less perturbed heat flux on the horizontal divertor target.

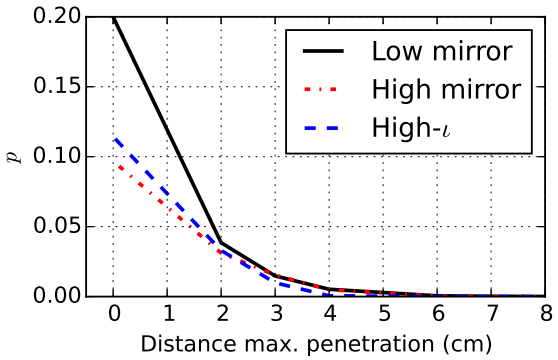


FIG. 11: Same as fig. 8 for the manipulator extending the horizontal target in the low mirror, high mirror, and high-$\iota$ configuration.

When analysing the power load on the manipulator for different penetration depth (fig. 11), two major aspects can be observed: firstly, although the magnetic topologies of the three cases compared are quite different the power fraction for different penetration depth shows a similar trend (only at maximum penetration depth it diverges). Secondly, the gradient (power fraction over penetration depth) is about a factor of five higher then in the case of a pumping gap manipulator. The divergence at maximum penetration depth of the low mirror configuration from the others results from the fact that the manipulator is already intersecting the LCFS in that configurations and therefore receives an increased amount of power load.

Based on this results the set-up appears very stable with respect to the predicted power load on the probe head at different configurations. Only drawback is the steeper power gradient. Ideally, it would be more flat to allow a finer adjustment of the received power load. However, this aspect can be compensated with a precise positioning system for the manipulator. Experimentally, one will insert the manipulator stepwise anyway.

Comparing the heat load redistribution on the divertor targets (fig. 12), one can observe

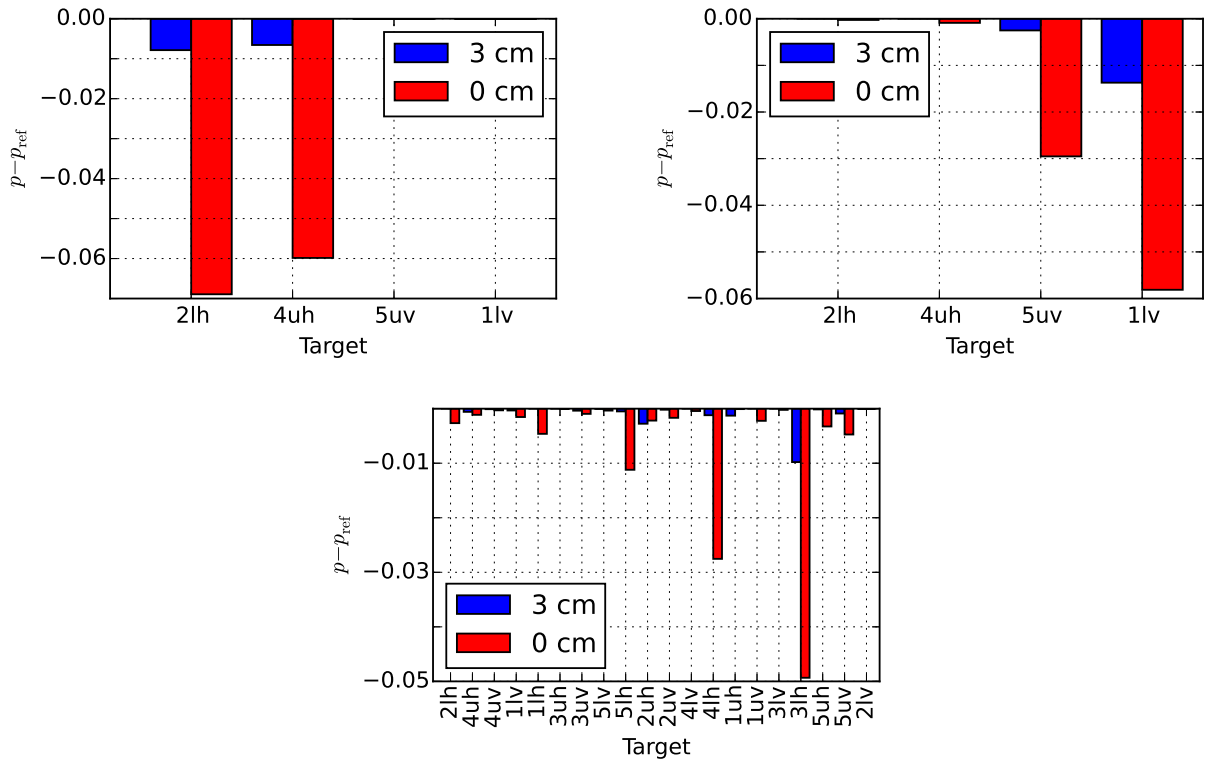


FIG. 12: Same as fig. 9 for the low mirror (top left), high mirror (top right), and high-$\iota$ (bottom) configuration in the case of a horizontal target extension manipulator.

in the mirror configuration a strong power load reduction at the horizontal (low mirror) or vertical (high mirror) targets. Compared to the set-up with a manipulator in the pumping gap a different island is intersected here, resulting in power load reduction on different targets. The contrast between the low and high mirror configuration can be easily understood when knowing that in each of the configurations only the horizontal or vertical targets are attached. Consequently, the intersecting manipulator can only reduce the power load on the horizontal or vertical targets. In the comparison with the pumping gap manipulator we find that the power reduction appears more symmetric on all targets intersected by the manipulator. A strong local effect like in the standard configuration with the manipulator in the pumping gap cannot be observed. Comparing the insertion up to the maximum position with a less deep insertion, one can notice a simple reduction of the redistributed power but a similar ratio between different targets. In high-$\iota$ configuration a power reduction on all lower horizontal targets can be observed where the total reduction is largest in the module toroidally before the manipulator (same as in the case with the pumping gap manipulator)

and decreases when following the island in toroidal direction. Generally, we can conclude that a horizontal target extension manipulator will cause a more symmetric power reduction on the divertor plates than a pumping gap manipulator, which might be simpler to operate with respect to real time power load control systems on the device.

With this set-up comparable heat fluxes to the real divertor plates are expected on the exposed material samples, if the probe head is sufficiently shaped and its vertical height carefully adjusted. The received heat and particle flux is to a certain extent controllable via the vertical manipulator position which can be used for power load scans of the sample materials.

### C. Mid-plane

The mid-plane manipulator is designed to reach across the LCFS into the confined region of the plasma. A consequence of the different magnetic configurations is the radial shift of the LCFS at mid-plane. This leads to an intersection of the mid-plane manipulator with the LCFS at different stroke depths, depending on the configuration. Obviously, the aspect is reflected in the power fraction received by the probe head at different penetration depths and configurations; see fig. 13. The grey vertical lines indicate the LCFS location along the probe path.

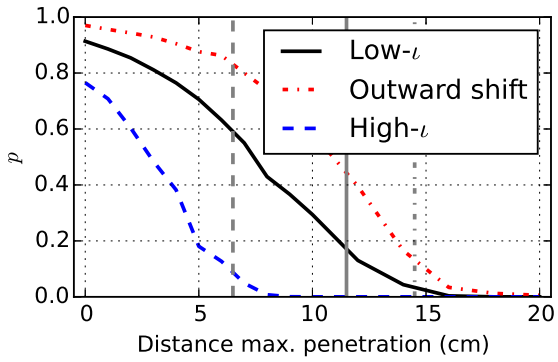


FIG. 13: Same as fig. 8 for the mid-plane manipulator in the low-$\iota$, outward shift, and high-$\iota$ configuration. The grey lines indicate the rough LCFS location.

The graph demonstrates clearly that a maximum penetration of the mid-plane manipulator is to no means foreseen for a standard plasma operation as the probe head would act

as the main limiter receiving all power. Equipped with Langmuir probes for plasma profile measurements one ideally would like to quickly plunge shortly inside the LCFS. From fig. 13 we know that such plunges need to be carefully adjusted as a similar plunge depth results in very different power loads depending on the magnetic configuration. The power gradient is even steeper than in the divertor manipulator set-ups. It varies slightly for different magnetic configurations and is about a factor of eight to 13 higher than in the manipulator set-up for the pumping gap. The mid-plane manipulator is designed for very fast plunges and will remain in the plasma only for about 100 ms to avoid severe damage. Typically, tungsten or molybdenum pins of electric probes require frequent exchange due to the high chance for melting under this conditions.

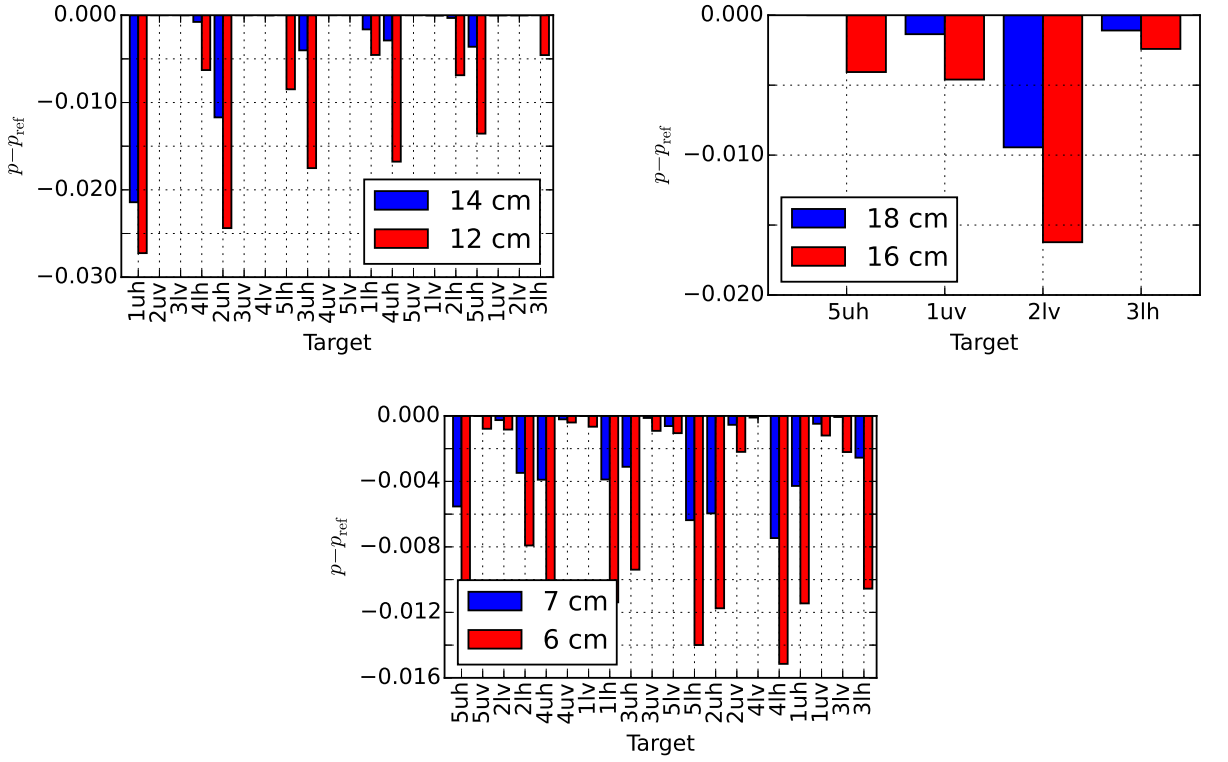


FIG. 14: Same as fig. 9 for the low-$\iota$ (top left), outward shift (top right), and high-$\iota$ (bottom) configuration in the case of the installed mid-plane manipulator.

It is interesting to know which parts of the divertor get shadowed due to the probe measurements at mid-plane for cross-checks with different diagnostics at remote locations. When inserting the probe head beyond the LCFS all divertor tiles will see a reduction of power load. Keeping the manipulator only in the island results in a power load reduction

at connected targets, as before. Figure 14 focuses on the second case only. In all three configurations we can observe that for the connected targets (island of low- and high-$\iota$ configuration is predominantly attached to the horizontal targets) a power reduction can be observed. The high-$\iota$ configuration shows an about equal amount of reduction on all targets (with some scatter). In the low-$\iota$ configuration one can notice a trend with the strongest reduction closed to the manipulator. The outward shift configuration shows the strongest reduction at a more remote location. This study makes clear that each case of interest need to be analysed separately and no general statement can be concluded here for the mid-plane manipulator. A detailed preparation for mid-plane probe experiments is needed to reduce the risk of damage and an thermography viewing system at the probe location is advisable.

## VI. CONCLUSIONS

Comparing the two divertor manipulator concepts one can conclude that each of the two does have different advantages over the other. Intersecting the divertor island from the pumping gap provides a less steep gradient in power load than penetrating from the bottom at the low-$\iota$ end of the horizontal target. However, due to a broader spread of the total power the manipulator acting as a horizontal target extension receives less heat flux and can cover a wider spatial range whereas the pumping gap manipulator is prone to overheating. The fact that three completely different magnetic topologies lead to a similar power load on the horizontal target extension manipulator can be seen as an advantage. It allows for a more direct comparison of effects due to the global change in magnetic topology while having similar power load conditions on the divertor.

The pumping gap manipulator allows in most magnetic reference configurations to reach near the divertor island centre which is excellent for the measurement of local plasma properties like electron temperature and density as well as streaming velocity near the divertor target. These are important input information for detailed SOL analysis and modelling. Locating a manipulator at the low-$\iota$ end as a toroidal extension of the horizontal target allows to reach at least six out of the nine magnetic reference configurations, in a horizontal divertor like manner. However, the limited availability of ports results in a geometrical restriction regarding the reachable region within the island. Only the outer strike-line of the island can be intersected with the current design. Still, for a steady-state exposure of

materials this appears as the reasonable option.

In contrast to the divertor manipulator the mid-plane manipulator is located in a less protected region. The heat flux gradient is about one order of magnitude steeper and a steady-state operation near the LCFS is risking a quick overheating of the probe head. Similar to the pumping gap manipulator the plasma intersection region varies a lot depending on the magnetic configuration which need to be taken into account when operating the mid-plane manipulator. Inserting the mid-plane manipulator fare beyond the LCFS will result in creating a main limiter with the probe.

This study summarises the properties of each set-up which need to be taken into account when exposing material samples or measuring plasma properties by utilising one of the manipulators. Ideally, one would couple all three manipulators with a thermography protections system that can control the quick retraction of the manipulators in case of overheating.

**Acknowledgments**

M.R. gratefully acknowledges the discussions with Dr. Y. Feng and comments by Dr. F. Schluck.

This work has been carried out within the framework of the EUROfusion Consortium and has received funding from the Euratom research and training programme 2014–2018 under grant agreement No 633053. The views and opinions expressed herein do not necessarily reflect those of the European Commission.

The authors gratefully acknowledge the computing time granted by the JARA-HPC Vergabegremium and VSR commission on the supercomputer JURECA at Forschungszentrum Jülich.

**Further simulation set-up**

The Wendelstein 7-X Webservices also provide a component and coil database that can serve as an input for the field line tracing service. Furthermore, components are grouped to assemblies and as part of the coil database full magnetic configurations are stored. In the presented studies all relevant components have been considered (assembly IDs in brackets): divertor units (2), baffle units (5), heat shields (6), toroidal closure units (7), full steel

panels for wall protection (8), full plasma vessel (9), and reduced steel panels without port / pumping slit protections (10). The magnetic configurations used all base on a vacuum approximation using the ideal Kisslinger coils (configuration IDs in brackets): standard (0), low-$\iota$ (3), high-$\iota$ (4), low mirror (5), high mirror (6), low shear (7), inward shift (8), outward shift (9), limiter (10). The considered manipulator probe heads base on CAD models.

---


[1] B. Schweer, S. Brezinsek, H. G. Esser, A. Huber, P. Mertens, S. Musso, V. Philipps, A. Pospieszczyk, U. Samm, G. Sergienko, et al., Fusion Science and Technology **47**, 138 (2005), URL http://www.new.ans.org/pubs/journals/fst/a_695.

[2] A. Herrmann, N. Jaksic, P. Leitenstern, H. Greuner, K. Krieger, P. de Marn, M. Oberkofler, V. Rohde, and G. Schall, Fusion Engineering and Design **98**, 1496 (2015), ISSN 0920-3796, proceedings of the 28th Symposium On Fusion Technology (SOFT-28), URL http://www.sciencedirect.com/science/article/pii/S0920379615000903.

[3] O. Neubauer, W. Biel, G. Czymek, P. Denner, F. Effenberg, A. Krmer-Flecken, Y. Liang, O. Marchuk, G. Offermanns, M. Rack, et al., Fusion Engineering and Design **96–97**, 891 (2015), ISSN 0920-3796, URL http://www.sciencedirect.com/science/article/pii/S0920379615301319.

[4] D. Nicolai, V. Borsuk, P. Drews, O. Grulke, K. Hollfeld, T. Krings, Y. Liang, C. Linsmeier, O. Neubauer, G. Satheeswaran, et al., Fusion Engineering and Design (2017), ISSN 0920-3796, URL http://www.sciencedirect.com/science/article/pii/S0920379617302168.

[5] G. Satheeswaran, K. Hollfeld, P. Drews, D. Nicolai, O. Neubauer, B. Schweer, and O. Grulke, Fusion Engineering and Design (2017), ISSN 0920-3796, URL http://www.sciencedirect.com/science/article/pii/S092037961730683X.

[6] P. Drews, Y. Liang, S. Liu, A. Kraemer-Flecken, O. Neubauer, J. Geiger, M. Rack, D. Nicolai, O. Grulke, N. Wang, et al., Nuclear Fusion (2017).

[7] Y. Feng, F. Sardei, and J. Kisslinger, Journal of Nuclear Materials **266-269**, 812 (1999), ISSN 0022-3115, URL http://www.sciencedirect.com/science/article/pii/S0022311598008447.

[8] *Eirene*, http://www.eirene.de, URL http://www.eirene.de.

[9] D. Reiter, M. Baelmans, and P. Börner, Fusion Science and Technology **47**, 172 (2005), URL

http://www.new.ans.org/pubs/journals/fst/a_698.

[10] T. Eich, D. Reiser, and K. Finken, Nuclear Fusion **40**, 1757 (2000), URL http://stacks.iop.org/0029-5515/40/i=10/a=307.

[11] S. Bozhenkov, J. Geiger, M. Grahl, J. Kilinger, A. Werner, and R. Wolf, Fusion Engineering and Design **88**, 2997 (2013), ISSN 0920-3796, URL http://www.sciencedirect.com/science/article/pii/S0920379613005711.

[12] J. Kißlinger, C. D. Beidler, E. Harmeyer, F. Rau, H. Renner, and H. Wobig, in *Proceeding of the 21st EPS Conference on Controlled Fusion and Plasma Physics* (1994), vol. 18B, p. 368.

[13] E. Strumberger, Contributions to Plasma Physics **38**, 106 (1998), ISSN 1521-3986, URL http://dx.doi.org/10.1002/ctpp.2150380115.

[14] J. D. Lore, T. Andreeva, J. Boscary, S. Bozhenkov, J. Geiger, J. H. Harris, H. Hoelbe, A. Lumsdaine, D. McGinnis, A. Peacock, et al., IEEE Transactions on Plasma Science **42**, 539 (2014), ISSN 0093-3813.

[15] T. Andreeva, Tech. Rep. IPP III/270, Max-Planck-Institut für Plasmaphysik, Garching (2002), URL http://hdl.handle.net/11858/00-001M-0000-0027-450D-A.